



HAL
open science

Matrix Product State Simulations of Non-equilibrium Steady States and Transient Heat Flows in the Two-Bath Spin-Boson Model at Finite Temperatures

Angus J Dunnett, Alex W. Chin

► **To cite this version:**

Angus J Dunnett, Alex W. Chin. Matrix Product State Simulations of Non-equilibrium Steady States and Transient Heat Flows in the Two-Bath Spin-Boson Model at Finite Temperatures. 2020. hal-03083803

HAL Id: hal-03083803

<https://hal.sorbonne-universite.fr/hal-03083803>

Preprint submitted on 19 Dec 2020

HAL is a multi-disciplinary open access archive for the deposit and dissemination of scientific research documents, whether they are published or not. The documents may come from teaching and research institutions in France or abroad, or from public or private research centers.

L'archive ouverte pluridisciplinaire **HAL**, est destinée au dépôt et à la diffusion de documents scientifiques de niveau recherche, publiés ou non, émanant des établissements d'enseignement et de recherche français ou étrangers, des laboratoires publics ou privés.

Article

Matrix Product State Simulations of Non-equilibrium Steady States and Transient Heat Flows in the Two-Bath Spin-Boson Model at Finite Temperatures

Angus J Dunnett ^{1*} and Alex W Chin ¹,

¹ Insitut des Nanosciences de Paris, Sorbonne Universit, CNRS, Place Jussieu, Paris, 75005

* Correspondence: angus.dunnett@insp.upmc.fr

Version December 19, 2020 submitted to Journal Not Specified

Abstract: Simulating the non-perturbative and non-Markovian dynamics of open quantum systems is a very challenging many body problem, due to the need to evolve both the system and its environments on an equal footing. Tensor network and matrix product states (MPS) have emerged as powerful tools for open system models, but the numerical resources required to treat finite-temperature environments grow extremely rapidly and limit their applications. In this study we use time-dependent variational evolution of MPS to explore the striking theory of Tamescelli et al. [1] that shows how finite-temperature open dyanmics can be obtained from zero temperature, i.e. pure wave function, simulations. Using this approach, we produce a benchmark data set for the dynamics of the Ohmic spin-boson model across a wide range of coupling and temperatures, and also present detailed analysis of the numerical costs of simulating non-equilibrium steady states, such as those emerging from the non-perturbative coupling of a qubit to baths at different temperatures. Despite ever growing resource requirements, we find that converged non-perturbative results can be obtained, and we discuss a number of recent ideas and numerical techniques that should allow wide application of MPS to complex open quantum systems.

Keywords: Open quantum systems, Tensor networks, non-equilibrium dynamics

1. Introduction

The physics of open quantum systems (OQS) plays a critical role in almost all aspects of quantum science [2,3], and the emergent phenomena of dephasing, decoherence and dissipation particularly limit our ability to initialise and control multi-partite quantum states. As a direct result of this, the development of scalable quantum technologies is greatly constrained by open system phenomena, and understanding how irreversibility arises from microscopic system-environment interactions has become essential for finding ways to mitigate deleterious noise effects [4]. However, alongside this goal of suppressing dissipative noise - normally by making the systems less 'open' - the theory of OQS also plays a vital role in the design of systems where the exploitation of *strong* energy and information exchange between a system and its environment is desirable: this is the world of quantum thermodynamics and nanoscale energy harvesting, storage and transduction [5–7].

Any 'machine' or device capable of converting *ambient* energy into work must necessarily be an open system. As these machines shrink to lengths where such energetic transformations can become few-quanta, ultra-fast events, it becomes necessary to describe their functional dynamics on timescales over which system-environment correlations - in both space and time - may be highly relevant [8,9]. Unlike the perturbative OQS found, for example, in atomic systems where dissipation can be characterised by simple decay rates, quantum energy harvesting naturally focuses on the highly non-Markovian and non-perturbative regime of OQS where the border between the 'system'

34 and ‘environment’ degrees of freedom is ill-defined. Moreover, as systems capable of converting
35 thermal energy must also reject a certain amount of heat to a colder reservoir [7], the study of quantum
36 energy harvesting leads directly to a consideration of multi-environment OQS, and the extended,
37 inter-environmental quantum correlations that could be generated under non-equilibrium operating
38 conditions.

39 Molecular and biological light-harvesting systems provide a good example of such nanoscale
40 energy extraction, in which a non-thermal population of electronic excitations (excitons, charge
41 pairs...) appears from the molecule-mediated connection of the ‘hot’ photon and ‘cold’ vibrational
42 environments. In this context, much attention has been placed on the complex physics due to the
43 strong coupling and non-separable timescales of electronic and environmental (vibrational) dynamics
44 [10–12], which include potentially exploitable effects such as transient breaking of detailed balance
45 [13], noise-induced electronic coherence and cooperative multi-environment effects [14,15]. In such
46 studies, the effect of light is normally assumed to be weak, leading to the ‘additive’ approximation
47 that phenomenological terms describing excitation, emission and dephasing can be simply added to
48 the more complex equations of motion of the vibronic open system. However, organic molecules often
49 have very strong light-matter coupling and can show surprising non-additive effects [16,17], including
50 nonlinear polaritonic weakening of exciton-phonon coupling in micro-cavity systems [18].

51 The example above highlights the theoretical challenges posed by some energy harvesting
52 systems: non-perturbative and highly structured couplings, comparable dynamical timescales and
53 competing environmental processes. Under these conditions the dissipative dynamics of the system’s
54 reduced density matrix cannot be simply described by dephasing and relaxation rates: the full
55 real-time evolution of the system and its environments must be accounted for on an essentially equal
56 footing. This looks, a priori, like a hopeless task, as each environment contains a continuum of
57 quantum excitation modes, and the formal number of quantum states in any computation will explode
58 exponentially with the number of such modes. However, things are not so desperate, and two broad
59 responses to this problem have emerged over recent years: one branch aims to efficiently simulate
60 the propagators of the system’s reduced density matrix [10,19–21], the other aims at representing
61 and evolving the entire system-environment wave function. Important contributions in this latter
62 domain are Density Matrix Renormalization Group (DMRG) techniques such as the Time Evolving
63 Density with Orthogonal Polynomials Approach (TEDOPA) [22,23], Dissipation-Assisted Matrix
64 Product Factorization [24], Time-Dependent Numerical Renormalisation Group techniques and the
65 Multi-Layer Multi Configurational Time-Dependent Hartree method (ML-MCTDH) developed in
66 Chemical physics [25,26].

67 The key to all of the wave function methods is the observation that, given a well-defined
68 initial condition, the quantum dynamics generated by typical system-environment Hamiltonians
69 leave the state inside a much smaller sub-space of the complete Hilbert space of the problem. This
70 suggests that the wave function can be parameterised by a potentially tractable number of parameters,
71 and - as we shall see - the effectively short-range, one-dimensional structure of OQS Hamiltonians
72 implies that Matrix Product States (MPS) will provide an efficient and versatile format for many
73 system-environment wave functions. Viewed this way, the parameters (matrices) of an MPS can be
74 considered as variational degrees of freedom, leading to the powerful 1-site time-dependent variational
75 principle (1TDVP) algorithm for efficient propagation of large wave functions in real-time [27]. This
76 general technique can be used in any MPS and Tree-Tensor Network problem [15], but it’s particular
77 utility in open-system problems has only recently been appreciated. We shall make use of this technique
78 in this article, but a discussion of MPS, TDVP and other computational aspects is left to the dedicated
79 presentations in the literature [27–30].

80 Instead, the key issue that we wish to explore in this study is the remarkable recent result of
81 Tamascelli *et al.* [1] that allows wave function approaches to OQS to effectively capture the effects of
82 *finite temperature* environments through the simulation of an equivalent *zero-temperature* proxy system.
83 As already discussed above, in the non-perturbative, non-Markovian regime of OQS, computing the

84 evolution of the single wave function from a sharp initial condition can already be very demanding:
 85 converging results over the astronomically large space of initial conditions in a thermal ensemble
 86 rapidly becomes impossible. If we also wish to explore the role of non-classical effects in heat flows
 87 *between* finite-temperature environments, the problem becomes exponentially worse. The access to
 88 finite temperature properties from a single zero-temperature (pure) wave function simulation thus
 89 opens up an entire class of powerful non-perturbative methods for the study of novel open quantum
 90 systems. This work aims to establish the extent to which Tamascelli's 'T-TEDOPA' theory translates
 91 into affordable non-perturbative TDVP simulations of thermal and non-equilibrium OQS dynamics, as
 92 well as to explore some of the non-classical and non-additive aspects of heat exchange in OQS.

93 This article is organised as follows. In Section 2.1 we present the spin-boson Hamiltonians that
 94 we will simulate. Sections 2.2 & 2.3 give a summary of the T-TEDOPA theory that we will employ
 95 in our numerical investigations. Section 2.4 then presents a careful study of the non-perturbative
 96 spin-boson model at finite temperatures which reveals some of the practical numerical costs implicit
 97 in this approach. Thanks to this testing, we are able to offer a freely accessible data set that can be used
 98 as a benchmark for other numerical approaches to this model, as well as code packages that allow
 99 users to perform their own TDVP calculations on finite-temperature open systems. In anticipation
 100 of the need to explore non-equilibrium states in a wide range of future contexts, we go on to test
 101 the non-perturbative physics of a two-level system (TLS) coupled to two environments at different
 102 temperatures in Section 2.5. Exploiting the information in the many-body system-environment(s)
 103 wave function, we examine the microscopic behaviour of the heat flows between the system and the
 104 environments as a function of environmental coupling strength and temperature differences, and
 105 highlight a number of non-additive effects arising from non-perturbative quantum polaron effects.
 106 Finally, we summarise and discuss our findings in Section 3.

107 2. Results

108 2.1. Model, parameters and initial conditions

109 We shall base our exploration of finite temperature open dynamics on numerical simulations and
 110 analysis of a quantum two-level system that is strongly coupled to either one or two baths of bosonic
 111 harmonic oscillators, as illustrated in Figure 1a. The two baths are labelled a and b and are at different
 112 inverse temperatures β_a and β_b , respectively ($\beta = 1/(k_b T)$). The system-bath Hamiltonian is given by

$$\hat{H} = \frac{\omega_0}{2} \sigma_z + \hat{H}_I^a + \hat{H}_I^b + \hat{H}_B^a + \hat{H}_B^b, \quad (1)$$

where

$$\hat{H}_I^a = \sigma_x \otimes \sum_k (g_k^* \hat{a}_k + g_k \hat{a}_k^\dagger) \quad (2)$$

$$\hat{H}_I^b = \sigma_x \otimes \sum_k (g_k^* \hat{b}_k + g_k \hat{b}_k^\dagger) \quad (3)$$

$$\hat{H}_B^a = \sum_k \omega_k \hat{a}_k^\dagger \hat{a}_k \quad (4)$$

$$\hat{H}_B^b = \sum_k \omega_k \hat{b}_k^\dagger \hat{b}_k. \quad (5)$$

113 The TLS is described by the standard Pauli operators σ , while the \hat{a}_k (\hat{b}_k) are bosonic annihilation
 114 operators for harmonic modes of frequency ω_k in bath a (b). The corresponding creation operators are
 115 denoted \hat{a}_k^\dagger (\hat{b}_k^\dagger). The k harmonic of each bath couples to the TLS with a coupling strength denoted g_k ,
 116 which we take to depend on the index k but not on a or b .

The spectral density of the environment is defined as $J(\omega) \equiv \pi \sum_k |g_k|^2 \delta(\omega - \omega_k)$, where $\delta(x)$ is the Heaviside Theta function. As a smooth, continuous function of frequency, the spectral density can

take various forms in specific physical realisations such as electron-phonon interactions, emitter-photon or exciton-vibration coupling in molecular systems. It is well known that the qualitative behaviour of the TLS depends sensitively on the form of $J(\omega)$, especially at low temperatures [19]. For simplicity, we assume identical system-bath couplings for both environments and use the common linear frequency dependence that defines an Ohmic environment ω_c

$$J(\omega) = 2\pi\alpha\omega\theta(\omega_c - \omega), \quad (6)$$

117 where α is a dimensionless coupling constant and we have introduced a hard frequency cut-off ω_c .

The initial condition $\hat{\rho}(0)$ for our numerical simulations is taken to be an uncorrelated (product) state of the spin and baths, which - because of the baths' finite temperatures - must be described by a mixed state, i.e. a density matrix

$$\hat{\rho}(0) = \rho_s \otimes \frac{e^{-\hat{H}_B^a \beta^a}}{\text{Tr}\{e^{-\hat{H}_B^a \beta^a}\}} \otimes \frac{e^{-\hat{H}_B^b \beta^b}}{\text{Tr}\{e^{-\hat{H}_B^b \beta^b}\}}, \quad (7)$$

118 where ρ_s is some arbitrary initial density matrix for the TLS.

119 Remarkably, despite the initial condition containing two statistically mixed thermal density
120 matrices, it has recently been shown by Tamascelli *et al.* that the reduced dynamics of the spin can still
121 be obtained from a *single* simulation of an equivalent *pure*, i.e. zero temperature, system-environment
122 wave function [1,31]. As this result is central for generating our numerical results and our later
123 discussion, we shall now give a brief summary of the protocol first presented in Ref. [1].

124 2.2. Finite-temperature reduced dynamics from pure wave function evolution

In this section we shall closely follow the original notation and presentation of Tamascelli *et al* [1] and, to simplify the presentation, we shall only consider the coupling to a single environment denoted E . The procedure can be easily generalised to multiple environments. Our starting point is the generic Hamiltonian for a system coupled to a bosonic environment consisting of a continuum of harmonic oscillators

$$H_{SE} = H_S + H_E + H_I, \quad (8)$$

where

$$H_I = A_S \otimes \int_0^\infty d\omega \hat{O}_\omega, H_E = \int_0^\infty d\omega \omega a_\omega^\dagger a_\omega. \quad (9)$$

The Hamiltonian H_S is the free system Hamiltonian and A_S is a generic system operator which couples to the bath. The Environment's free Hamiltonian is given by H_E . For the bosonic bath operators we take the displacements

$$O_\omega = \sqrt{J(\omega)}(a_\omega + a_\omega^\dagger), \quad (10)$$

125 thus defining the spectral density $J(\omega)$. This has been written here as an arbitrary continuous function,
126 but we note that the formulas can also be applied to the case of coupling to a discrete set of vibrational
127 modes by adding suitable structure to the spectral density, i.e. sets of lorentzian peaks or Dirac
128 functions [32–34].

129 The state of the system+environment at time t is a mixed state described by a density matrix
130 $\rho_{SE}(t)$. The initial condition is assumed to be a product of system and environment states $\rho_{SE}(0) =$
131 $\rho_S(0) \otimes \rho_E(0)$ where $\rho_S(0)$ is an arbitrary density matrix for the system and $\rho_E(0) = \exp(-H_E \beta) / \mathcal{Z}$,
132 with the environment partition function given by $\mathcal{Z} = \text{Tr}\{\exp(-H_E \beta)\}$. Such a product state is
133 commonly realised in non-equilibrium problems where the system is suddenly prepared or projected
134 into an excited state from a ground state in which the system and environment states are separable.
135 This type of preparation is exemplified by the Franck-Condon principle in molecular photophysics,
136 where the optical transition occurs without any change in the nuclear degrees of freedom, leaving the
137 subsequent relaxation dynamics to evolve from a product 'initial' condition [35,36]. The environment

138 thus begins in a thermal equilibrium state with inverse temperature β , and the energy levels of each
 139 harmonic mode are statistically populated. For a very large number (continuum) of modes, the number
 140 of possible thermal configurations grows extremely rapidly with temperature, essentially making
 141 it impossible to obtain a converged sampling of these configurations when each instance involves
 142 demanding wave function simulations. We briefly note that some more efficient sampling methods
 143 involving sparse grids and/or stochastic mean-field approaches have recently been proposed and
 144 demonstrated [37,38], as well as some effective MPS techniques for capturing finite temperature effects
 145 in frequency domain simulations [39].

The initial thermal condition of the environmental oscillators is also a Gaussian state, for which it is further known that the influence functional [2] - which is a full description of the influence of the bath on the system - will depend only on the two-time correlation function of the bath operators

$$S(t) = \int_0^\infty d\omega \langle O_\omega(t) O_\omega(0) \rangle. \quad (11)$$

146 Any two environments with the same $S(t)$ will have the same influence functional and thus give rise
 147 to the same reduced system dynamics, i.e. the same $\rho_S(t) = \text{Tr}\{\rho_{SE}(t)\}$. That the reduced density
 148 matrix's dynamics are completely specified by the spectral density and temperature of a Gaussian
 149 environment has been known for a long time [2], but the key idea of the equivalence - and thus the
 150 possibly of the interchange - of environments with the same correlation functions has only recently
 151 been demonstrated by Tamascelli *et al.* [31].

The time dependence in eq. 11 refers to the interaction picture so that the bath operators evolve under the free bath Hamiltonian: $O_\omega(t) = e^{iH_E t} O_\omega(0) e^{-iH_E t}$. Using eq. 10 and $\langle a_\omega^\dagger a_\omega \rangle = n_\beta(\omega)$ we have

$$S(t) = \int_0^\infty J(\omega) [e^{-i\omega t} (1 + n_\beta(\omega)) + e^{i\omega t} n_\beta(\omega)]. \quad (12)$$

Making use of the relation

$$\frac{1}{2}(1 + \coth(\omega\beta/2)) \equiv \begin{cases} n_\omega(\beta), \omega \geq 0 \\ -(n_{|\omega|}(\beta) + 1), \omega < 0 \end{cases} \quad (13)$$

we can write eq. 12 as an integral over all positive and negative ω

$$S(t) = \int_{-\infty}^\infty d\omega \text{Sign}(\omega) \frac{J(|\omega|)}{2} (1 + \coth(\frac{\omega\beta}{2})) e^{-i\omega t}. \quad (14)$$

But eq. 14 is exactly the two-time correlation function one would get if the system was coupled to a bath, now containing positive and negative frequencies, at zero temperature! The effects of the finite, physical temperature now appear in a new effective spectral density for the extended environment given by

$$J_\beta(\omega) = \text{Sign}(\omega) \frac{J(|\omega|)}{2} (1 + \coth(\frac{\omega\beta}{2})). \quad (15)$$

Thus, we find that our open system problem is completely equivalent to the one governed by the Hamiltonian

$$H = H_S + H_E^{\text{ext}} + H_I^{\text{ext}}, \quad (16)$$

in which the system couples to an extended environment, where

$$\begin{aligned} H_I^{\text{ext}} &= A_S \otimes \int_{-\infty}^\infty d\omega \sqrt{J_\beta(\omega)} (a_\omega + a_\omega^\dagger), \\ H_E^{\text{ext}} &= \int_{-\infty}^\infty d\omega \omega a_\omega^\dagger a_\omega, \end{aligned} \quad (17)$$

152 and which has the initial condition $\rho_{SE}(0) = \rho_S(0) \otimes |0\rangle_E \langle 0|$. This transformed initial condition is now
 153 far more amenable to simulation as the environment is now described by a *pure*, single-configuration
 154 wave function, rather than a statistical mixed state, and so *no* statistical sampling is required to capture
 155 the effects of temperature on the reduced dynamics!

156 Analysing the effective spectral density of Eq. 15, it can be seen that the new extended environment
 157 has thermal detailed balance between absorption and emission processes encoded in the ratio of the
 158 coupling strengths to the positive and negative modes in the extended Hamiltonian (see Figure 1c), as
 159 opposed to the operator statistics of a thermally occupied *state* of the original, physical mode, i.e.

$$\frac{J_\beta(\omega)}{J_\beta(-\omega)} = \frac{\langle a_\omega a_\omega^\dagger \rangle_\beta}{\langle a_\omega^\dagger a_\omega \rangle_\beta} = e^{\beta\omega} \quad (18)$$

160 Indeed, from the system's point of view, there is no difference between the absorption of a
 161 quantum from a thermally occupied, positive energy bath mode and the creation (emission) of an
 162 excitation into an unoccupied, negative energy, bath mode. The extension to negative frequencies
 163 essentially allows the process whereby the system would be heated by the environment (absorbing
 164 pre-existing quanta in the thermal bath) to be mimicked by spontaneous emission into a negative
 165 energy vacuum of states, as shown in Figure 1b.

166 In fact, the equivalence between these two environments goes beyond the reduced system
 167 dynamics as there exists a unitary transformation which links the extended environment to the original
 168 thermal environment. This means that one is able to reverse the transformation and calculate thermal
 169 expectations for the actual bosonic bath such as $\langle a_\omega^\dagger(t) a_\omega(t) \rangle_\beta$. This is particularly useful for molecular
 170 systems in which environmental (vibrational) dynamics are also important observables that report on
 171 the mechanisms and pathways of physio-chemical transformations [40–42]. In this article, we will use
 172 this capability later to look at the non-equilibrium heat flows between the TLS and its environments.
 173 This is a major advantage of many-body wave function approaches, as full information about the
 174 environment is available, cf. effective master equation descriptions which are obtained *after* averaging
 175 over the environmental state.

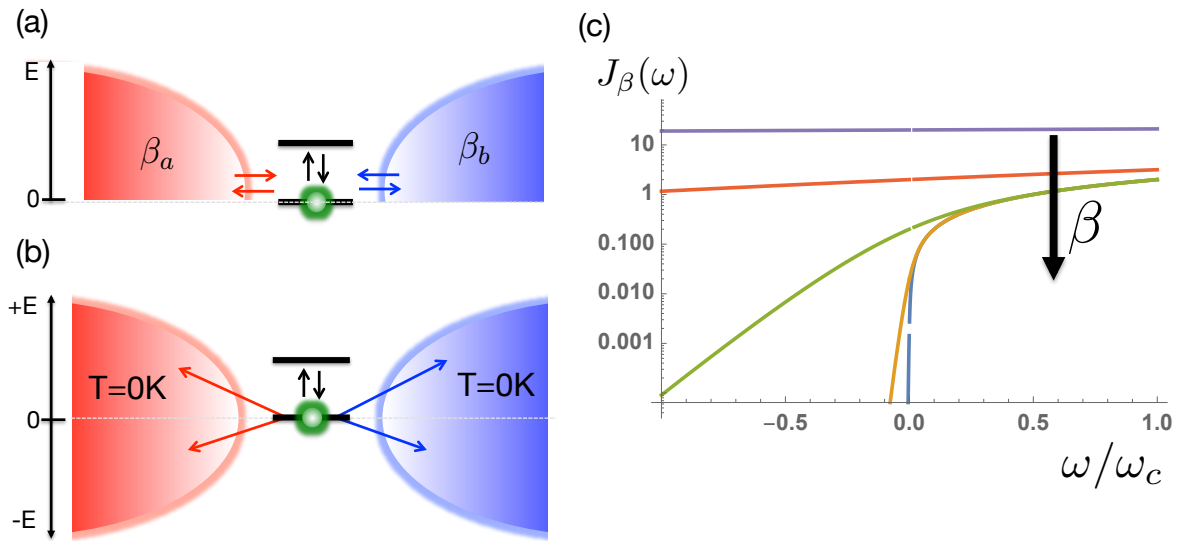


Figure 1. (a) Two-level system (TLS) is coupled to two environments (a, b) with inverse temperatures β_a and β_b . (b) The reduced state dynamics of the TLS can be obtained from a zero-temperature simulation of an extended environment containing negative frequency excitation modes and temperature-dependent couplings. (c) The effective spectral density $J_\beta(\omega)$ encodes the principle of detailed balance for absorption and emission of quanta between thermal transitions in the TLS. For the Ohmic spectral density considered in this article, $J_\beta(\omega)$ becomes flat over the entire range $[-\omega_c, \omega_c]$ as the temperature increases (β decreases). The plots shown are for $\omega_c \beta = 0.1$ (Purple), $\omega_c \beta = 1$ (Red), $\omega_c \beta = 10$ (Green), $\omega_c \beta = 50$ (Yellow) and $\omega_c \beta = 100$ (Blue).

176 2.3. Chain mapping and chain coefficients

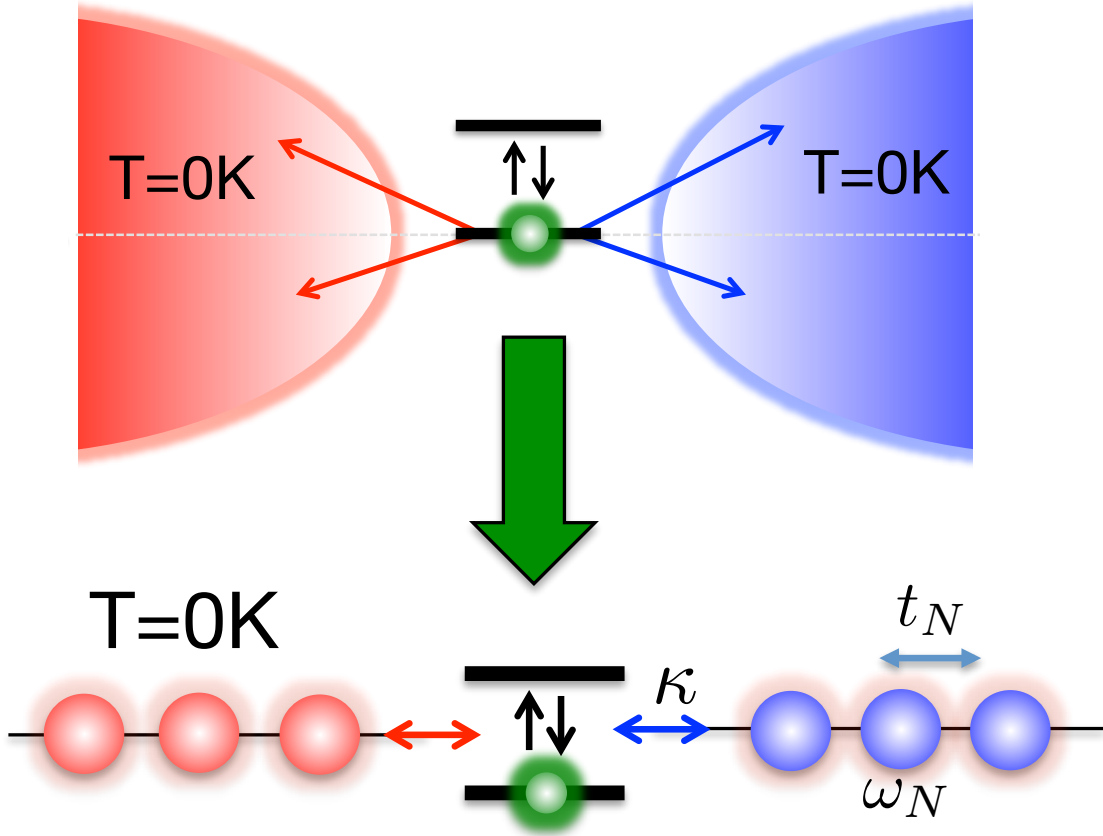


Figure 2. The positive and negative energy modes of each extended environment are mapped onto 1D chains with nearest-neighbour hopping, each coupled by their first site to the TLS with coupling strength κ . The chain parameters ϵ_n and t_n are determined such that the eigen-modes of the chains are the original modes of the extended environments. The 1D geometry of the transformed system and the fact that the chain modes all start in their vacuum states, means the system-environment state can be described by a single (pure) MPS.

Following this transformation a further step is required to facilitate efficient simulation of the many-body system+environment wave-function. This is to apply a unitary transformation to the bath modes which converts the *star-like* geometry of H_I^{ext} into a *chain-like* geometry, thus allowing the use of Matrix-Product-State (MPS) methods [11,43,44] (see Figure2). We thus define new modes $c_n^{(\dagger)} = \int_{-\infty}^{\infty} U_n(\omega) a_{\omega}^{(\dagger)}$, known as chain modes, via the unitary transformation $U_n(\omega) = \sqrt{J_{\beta}(\omega)} p_n(\omega)$ where $p_n(\omega)$ are orthonormal polynomials with respect to the measure $d\omega J_{\beta}(\omega)$. Thanks to the three term recurrence relations associated with all orthonormal polynomials $p_n(\omega)$ [43], only one of these new modes, $n = 1$, will be coupled to the system, while all other chain modes will be coupled only to their nearest neighbours [43]. Our interaction and bath Hamiltonians thus become

$$\begin{aligned}
 H_I^{\text{chain}} &= \kappa A_S (c_1 + c_1^{\dagger}), \\
 H_E^{\text{chain}} &= \sum_{n=1}^{\infty} \epsilon_n c_n^{\dagger} c_n + \sum_{n=1}^{\infty} (t_n c_n^{\dagger} c_{n+1} + h.c.).
 \end{aligned}
 \tag{19}$$

177 The chain coefficients appearing in eq. 19 are related to the three-term recurrence parameters of the
 178 orthonormal polynomials and can be computed using standard numerical techniques [43]. Since the
 179 initial state of the bath was the vacuum state, it is unaffected by the chain transformation. We briefly

180 note the evolution of the asymptotic values of the chain parameters, as illustrated in Figure 3. For a
181 smooth spectral density with a hard cut-off, it has been rigorously proven that $\epsilon_n \rightarrow \omega_c/2, t_n \rightarrow \omega_c/4$
182 as $n \rightarrow \infty$ [45]. Figure 3 shows the dramatic changes in these asymptotic values as the temperature
183 is increased, which - from the numerical results - appear to be $\epsilon_n \rightarrow 0, t_n \rightarrow \omega_c/2$ as $n \rightarrow \infty$ and
184 $\beta \rightarrow 0$. This can be naturally understood from the behaviour of the effective spectral functions $J_\beta(\omega)$
185 with increasing temperature, as illustrated in Figure 1c. The spectral functions become symmetric and
186 have finite values over the whole domain $[-\omega_c, \omega_c]$. The asymptotic spectrum of the chain modes
187 thus has a bandwidth of $2\omega_c$ centred on $\omega = 0$, which, for a uniform hopping chain, requires the
188 numerically observed asymptotic chain parameters. In the particular case of the Ohmic environment
189 at high temperatures, it can easily be seen that $J_\beta(\omega)$ tends to a constant and so will have a chain
190 representation derived from the classical Legendre polynomials [45].

191 We have thus arrived at a formulation of the problem of finite-temperature open systems in which
192 the many-body environmental state is initialised as a pure product of trivial ground states, whilst
193 the effects of thermal fluctuations and populations are encoded in the Hamiltonian chain parameters
194 and system-chain coupling. These parameters must be determined once for each temperature but
195 - in principle - the actual simulation of the many-body dynamics is now no more complex than a
196 zero-temperature simulation!

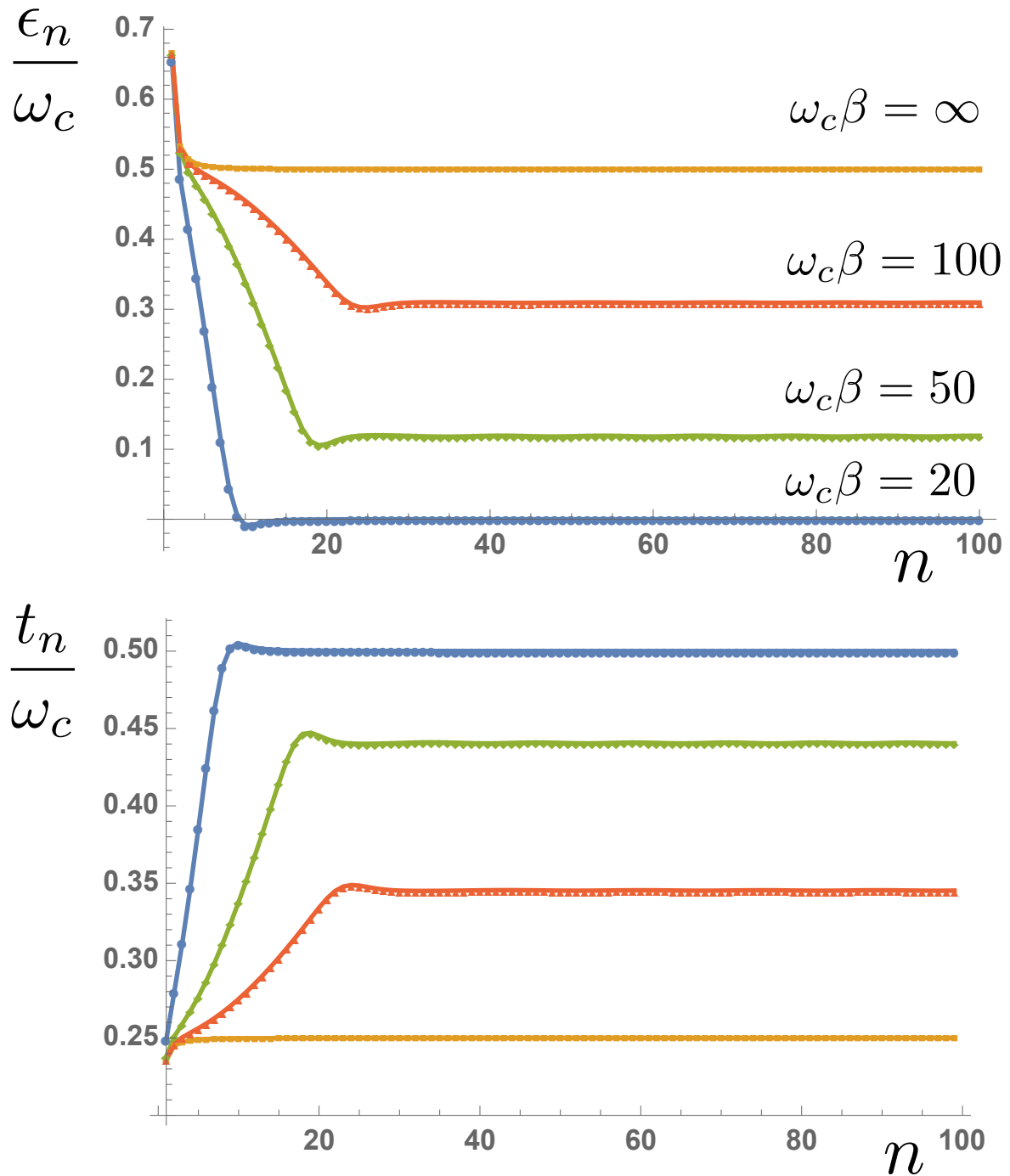


Figure 3. Site energies e_n (a) and hopping amplitudes t_n (b) as a function of chain distance n at different environment temperatures

197 2.4. Spin-boson model across the complete $\alpha - \beta$ space

198 In this section, we numerically verify that the finite-temperature approach set out in Sections
 199 2.2 & 2.3 captures the correct non-perturbative behaviour in the single-bath spin-boson model. This
 200 will be illustrated with a few explicit examples, but the key result of this section is the creation of a
 201 comprehensive data set for the Ohmic spin-boson model that allows arbitrary TLS initial conditions to
 202 be propagated in real-time and over a large area of $\alpha - \beta$ space. This data set has been made freely
 203 available online in citable form and can be used to benchmark other methods and applications [46].

204 Figure 4a,b shows the temporal decay of an initially polarised spin $\langle \sigma_z(0) \rangle = +1$ towards thermal
 205 equilibrium for varying coupling strengths α and inverse temperatures β . The TLS energy splitting

206 was $\omega_0 = 0.2\omega_c$. The key result in Figure 4b is the dependence of the thermalized spin polarization at
 207 long times. In a simple, perturbative rate equation treatment, this final polarization would be set by
 208 the energy gap ω_0 and the temperature, according to the Gibbs-Boltzmann distribution

$$\langle\sigma_z\rangle_\beta = -\frac{(1 - e^{-\beta\omega_0})}{(1 + e^{-\beta\omega_0})}. \quad (20)$$

209 The coupling strength α would only alter the rate at which this thermal distribution is reached.
 210 However, Figure 4a shows a growing dependence of the final polarization on the coupling strength,
 211 suggesting a non-perturbative effect. This is indeed the case: strong coupling leads to polaron
 212 formation and non-perturbative renormalisation of the TLS energy gap ω_0 . According to the variational
 213 theory of Silbey and Harris [47], the renormalized gap ω_r is approximately given by

$$\omega_r = \omega_0 \left(\frac{\omega_0}{\omega_c}\right)^{\frac{\alpha}{1-\alpha}}, \quad (21)$$

in the so-called scaling limit in which ω_c is much larger than all other energy scales in the problem.
 This renormalisation is highly non-perturbative, and can completely close the TLS energy gap at a
 critical coupling $\alpha_c = 1$ [2]. Replacing ω_0 with the the renormalized energy gaps in Eq. 20, $\langle\sigma_z\rangle_\beta$ is
 given

$$\langle\sigma_z\rangle_\beta = -\left(\frac{\omega_0}{\omega_c}\right)^{\frac{\alpha}{1-\alpha}} \frac{(1 - e^{-\beta\omega_r})}{(1 + e^{-\beta\omega_r})}. \quad (22)$$

214 where the prefactor in accounts for the suppressed expectation values of σ_z in the polaronic eigenbasis.

215 Figure 5 shows this analytical prediction as a function of temperature, compared to the results
 216 extracted from the real-time dynamics. As mentioned above, most analytical predictions for the SBM
 217 are obtained deep in the scaling limit, while numerical results necessarily involve only moderately
 218 large values of ω_c . When comparing results, it is common in the literature to evaluate analytical
 219 expressions with a re-scaled coupling strength $\tilde{\alpha} = c\alpha$ to account for this [48–50], which we have
 220 applied in Figure 5. We found that a constant factor $c = 0.66$ gave excellent agreement across the
 221 parameter space for both one and two-bath SBMs, as shown in the inset of Figure 5.

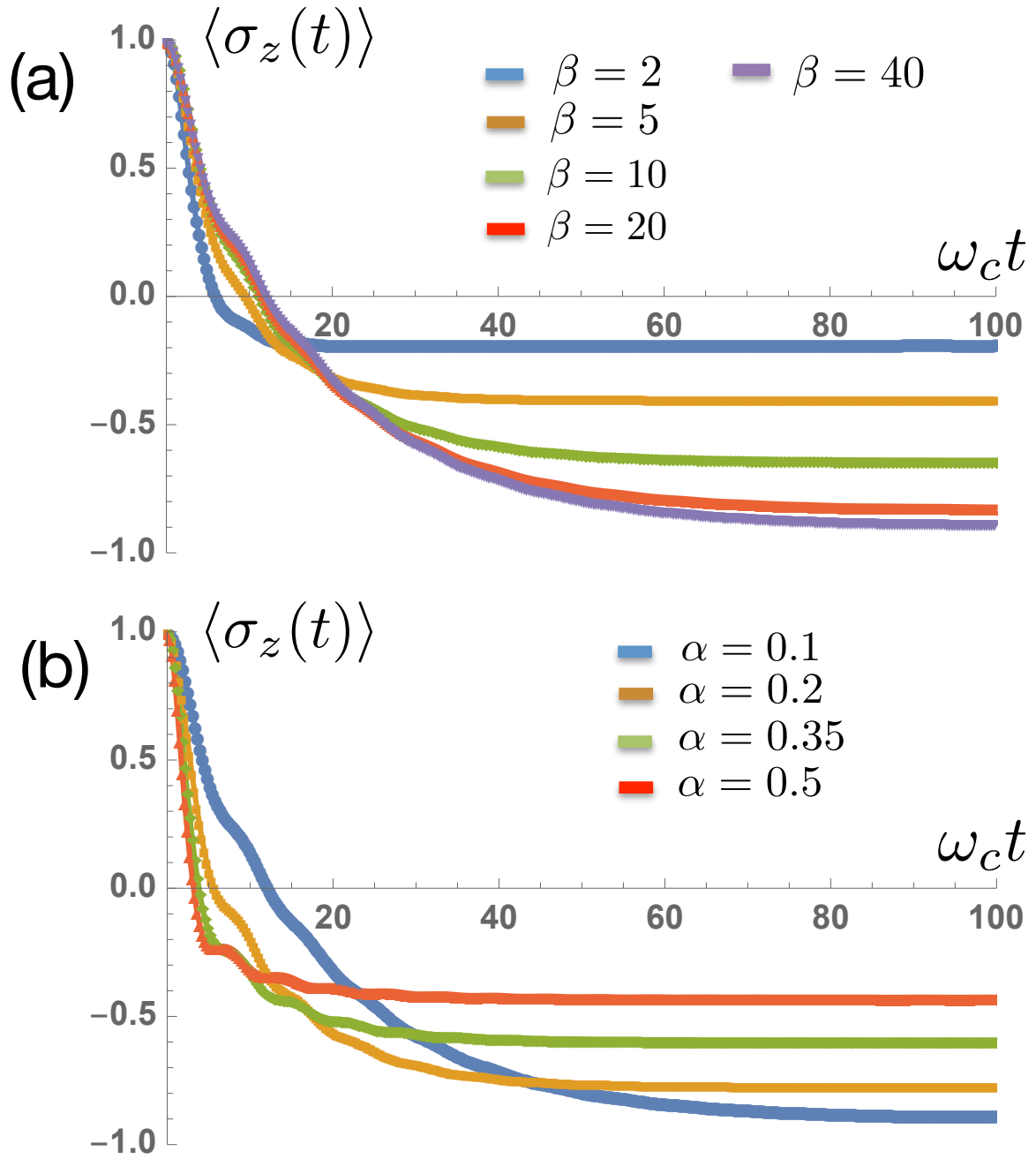


Figure 4. Relaxation of spin polarization as a function of time for (a) different temperatures and $\alpha = 0.1$ and (b) different coupling strengths with a fixed $\omega_c \beta = 100$.

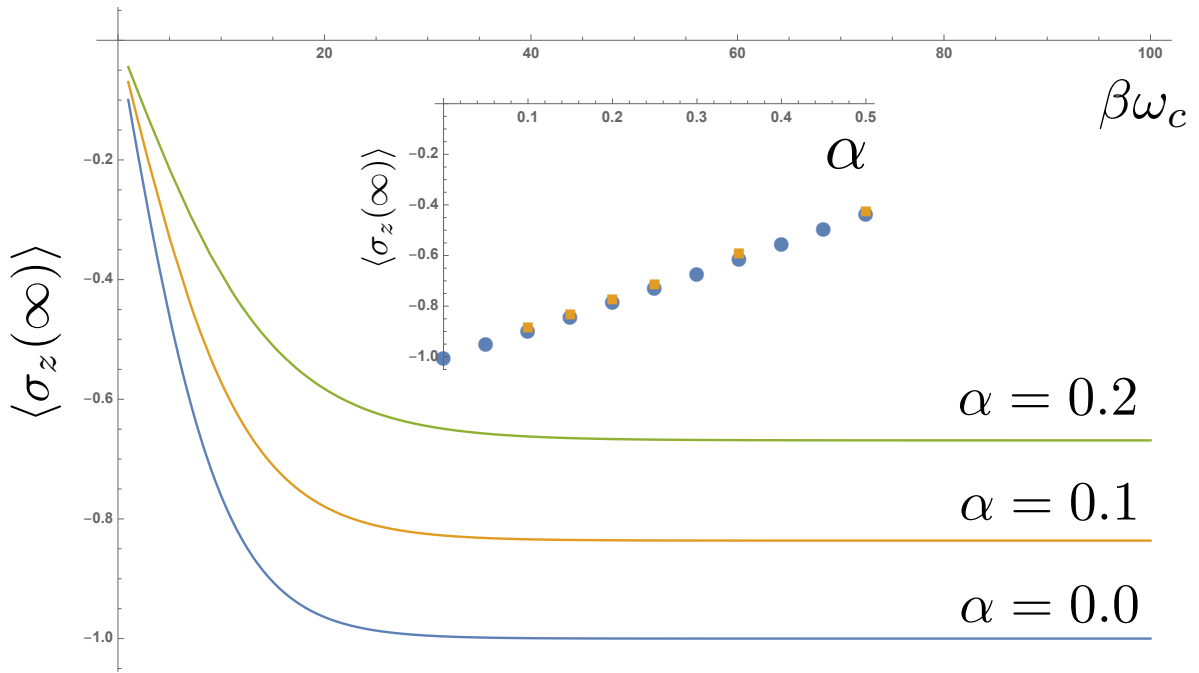


Figure 5. Analytical prediction of thermal steady state spin polarization as a function of inverse temperature $\omega_c\beta$. Inset compares these predictions with steady state values extracted from the real-time dynamics shown in Figure 4. A re-scaled coupling strength $\tilde{\alpha} = c\alpha$ with $c = 0.66$ has been applied when evaluating the analytical formula (see main text).

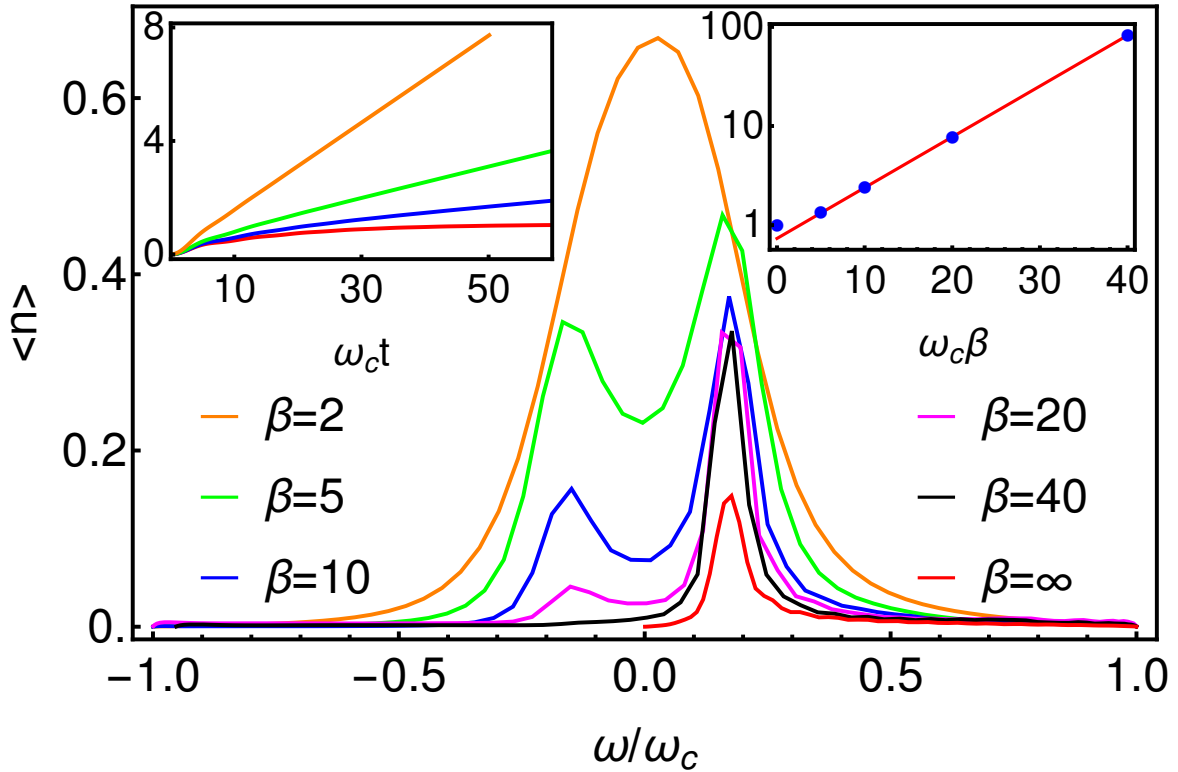


Figure 6. Long-time occupations of the modes of the extended environment, following the thermalization of the TLS at various temperatures. Inset shows the total number of quanta in the environment as a function of time (left) for different temperatures. This population grows indefinitely at finite temperatures. The inset (right) shows the long-time ratio of the peak heights in each curve of the main figure. These give a very good fit to the exponential dependence expected for absorption and emission rates obeying detailed balance.

222 As a final set of observations in this section, we now look at the behaviour of the environment. In
 223 Figure 6 we present the occupations of the bath modes in the extended spectral representation used
 224 to account for finite temperatures. As anticipated in our discussion in Section 2.2, we find that at
 225 low temperatures, the energy released from the decay of the spin is absorbed by modes with positive
 226 frequencies matching the TLS energy gap ω_0 . As the temperature increases, peaks appear at negative
 227 frequencies, corresponding to the excitation of these modes due to ‘heating’ of the TLS, i.e. the TLS
 228 is thermally excited and removes energy from the environment. As a function of temperature, the
 229 ratio of the positive and negative occupations is a very close fit to $e^{\beta\omega_0}$, as expected from detailed
 230 balance. However, due to the presence of negative frequency modes, we find that the populations
 231 in *both* the positive and negative frequency modes grow *indefinitely* during the simulation time, as
 232 shown in the inset of Figure 6. The difference of these growing populations plateaus at a finite value,
 233 corresponding to the thermal occupation of the physical positive-frequency mode, but care must be
 234 taken to get converged results for long-time (steady state) quantities due to the expanding local Hilbert
 235 spaces needed for the environment modes in the simulations.

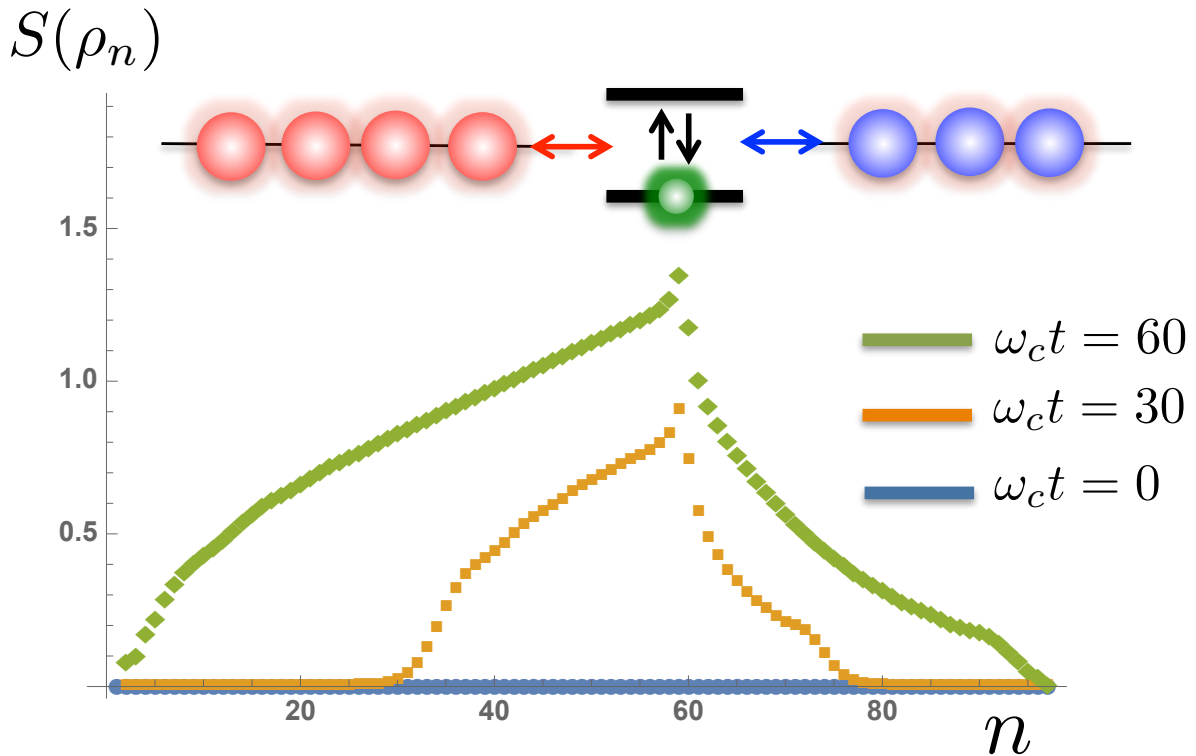


Figure 7. The time evolution of the von Neumann entanglement entropy for each bi-partition of the system-environment chain at site n . The TLS is located in this example at site $n = 59$, with the hot bath corresponding to sites 1 – 58 and remaining sites represent the cold bath.

236 Figure 7 shows the behaviour of the von-Neumann entropy obtained by bi-partitioning the total
 237 N -site system-environment chain into chains of size n and $N - n$ and computing the singular values
 238 of either of the subsystems' reduced density matrices [51]. The entanglement entropy directly reports
 239 on the size of the bond-dimensions required to represent the state accurately in the MPS format, and
 240 our results show that this entropy also grows continuously during the simulation. There is also a clear
 241 asymmetry in the rate of spreading and magnitudes of entanglement, with correlations between sites
 242 in the hot environment growing much faster. Again, these growing numerical resources for finite
 243 temperature simulations should be handled with care, and we shall take this up again in Section 3.

244 2.5. Non-equilibrium heat flows

245 In this section we simulate the non-equilibrium dynamics of the TLS connected to two
 246 environments at different temperatures. For clarity we will designate environment a as the 'hot'
 247 environment and b as the 'cold' one, using suffixes 'c' and 'h', respectively. We note here that this
 248 elementary class of two-environment models has both wide-ranging practical applications - such
 249 as studying heat and charge transfer in nano-devices and molecules [7,52,53], as well as being of
 250 fundamental relevance for quantum thermodynamics, decoherence, and non-equilibrium steady states
 251 [54–58].

Figure 8 shows the real-time excitation of a TLS initially prepared in its ground state when connected at $t = 0$ to the cold environment with fixed $\omega_0\beta_c = 100$ and the 'hot' environment at different temperatures. Figure 9 shows the steady-state spin polarization as a function of the temperature difference between the hot and cold baths. To understand the basic features of the steady state, let's consider a perturbative set of rate equations for the population of the spin-up level $P_{\uparrow}(t)$.

Assuming that the rates of absorption and emission from each bath of TLS obey detailed balance, the dynamics of $P_{\uparrow}(t)$ can be obtained from the equation

$$\frac{dP_{\uparrow}(t)}{dt} = -\Gamma P_{\uparrow}(t)(n_c + n_h + 2) + \Gamma(1 - P_{\uparrow}(t))(n_c + n_h), \quad (23)$$

where $n_i = [\exp(\omega_0\beta_i) - 1]^{-1}$. By finding the steady state population $P_{\uparrow}(\infty)$, the non-equilibrium value of the spin polarisation $\langle\sigma_z^{ab}(\infty)\rangle$ then takes the simple form

$$\langle\sigma_z^{ab}(\infty)\rangle = \frac{-1}{2(n_c + n_h + 1)}. \quad (24)$$

252 Once again, if renormalization effects are included, the agreement between the analytical predictions
 253 is very good, as can be seen in Figure 9. Indeed, for the lowest temperatures, the spin dynamics are
 254 entirely due to renormalization effects, as thermal occupation of the excited level is negligible.

255 Interestingly, these two-bath results also reveal an intriguing non-additive effect due to the
 256 coupling to two environments. The subject of non-additivity of environmental interactions has recently
 257 attracted attention due to the role of multiple environments in a wide range of ‘active’ quantum
 258 machines, such as the conversion of ambient solar energy in room-temperature (phonon-coupled)
 259 devices [16,17,50], and also the highly co-operative actions of different types of vibrational motion
 260 in molecular photo physics [15]. In the present case, the non-additive effects appear in the polaronic
 261 renormalisation, which is mostly clearly seen in the case when the two baths have the same temperature.
 262 This situation is indistinguishable from a coupling to a single bath with twice the coupling strength.
 263 The renormalisation can thus be obtained from Eq. 21 with the replacement $\alpha \rightarrow 2\alpha$. However, the
 264 renormalisation arises from the overlap of the displaced mode wave functions that are ‘fast’ enough to
 265 co-tunnel with the TLS as it transitions between $\langle\sigma_x\rangle = \pm 1$ [47,48], and in an additive approximation
 266 the renormalization would be simply be the product of the individual overlaps for each environment.
 267 However, as is clear from Eq. 21, this doubling of the coupling does not lead to a simple exponential
 268 doubling of the renormalization, but instead leads to a nonlinear suppression of the energy gap
 269 according to the exponent $2\alpha/(1 - 2\alpha)$.

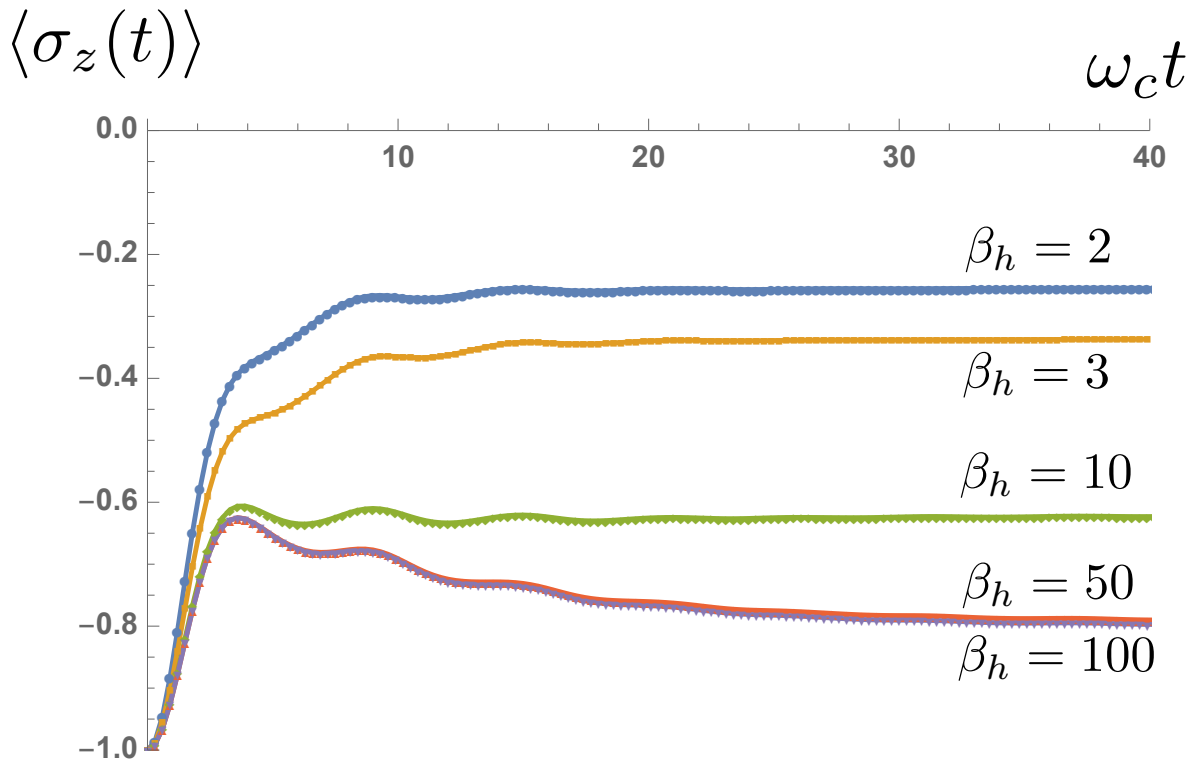


Figure 8. Non-equilibrium relaxation of spin polarization as a function of time for fixed cold bath temperature and varying hot bath temperatures.

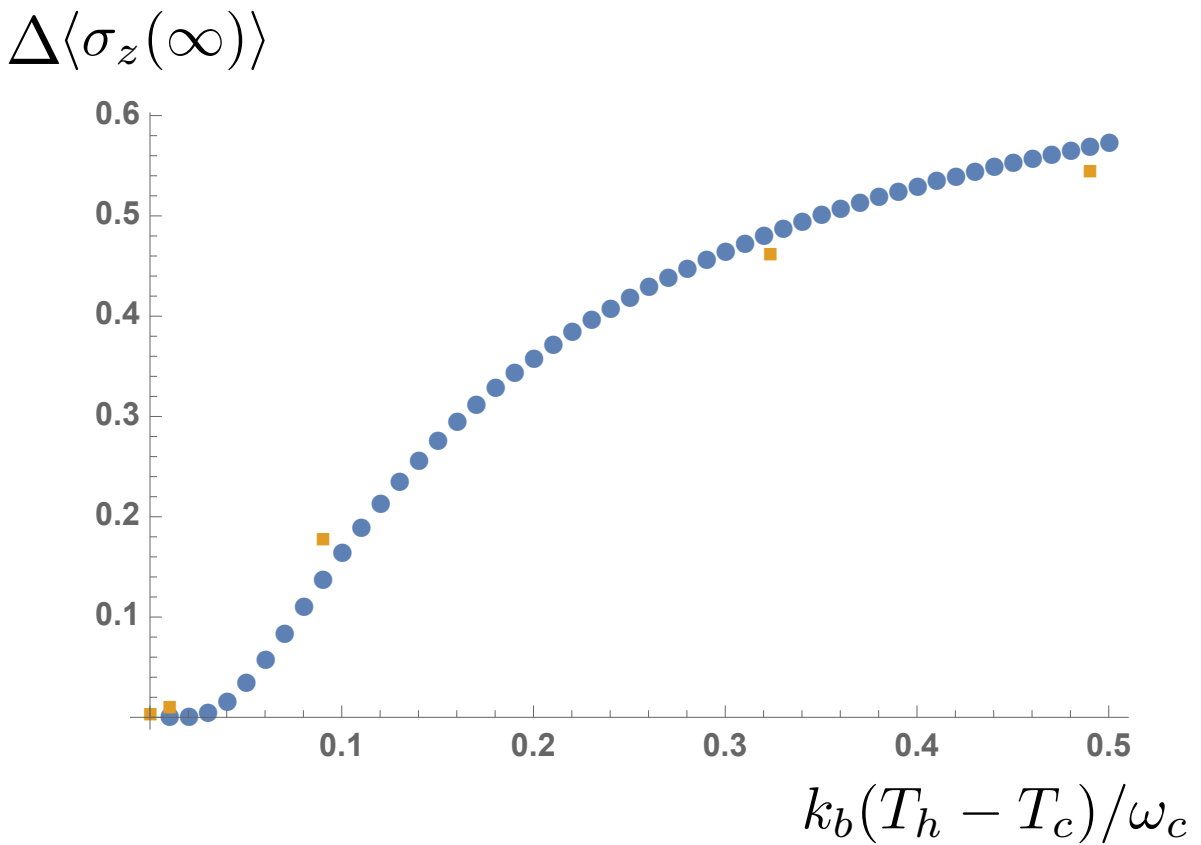


Figure 9. The change in $\langle \sigma_z(\infty) \rangle$ as a function of the temperature difference between the baths (T_c is kept constant). Analytical predictions are shown as dots, numerical data points as squares.

Exploiting the access to the environmental state, we now show the transient dynamics of the heat flow in the two baths during the establishment of the TLS steady state. We define the following operators

$$\hat{J}_c = \hat{\sigma}_y \otimes (\hat{A}_0^\dagger + \hat{A}_0), \quad (25)$$

and

$$\hat{J}_h = \hat{\sigma}_y \otimes (\hat{B}_0^\dagger + \hat{B}_0), \quad (26)$$

which measure the heat flux from the spin to baths *a* and *b* respectively. Representative heat flows are shown in Figure 10 for large and zero differences in the bath temperatures. In both cases, the initial dynamics involve heating from *both* hot and cold environments, as the spin is initially in a pure ($T = 0K$) ground state. As the dynamical steady state of the spin is obtained, a net heat current appears from the hot to cold environment. This heat current vanishes as the temperature difference of the baths is reduced, as we would expect. From the long-time solution of the Pauli master equation given in Eq. 23, the steady-state heat flux from the hot to cold environment can be shown to be

$$J = \Gamma \frac{n_h - n_c}{1 + n_h + n_c}, \quad (27)$$

270 and this is plotted alongside our numerical data in Figure 11. The simulations correctly capture the
 271 essentially non-linear behaviour of heat flow through the quantum ‘heat leak’ TLS, although a linear
 272 regime where Fourier’s law of heat flow appears to hold can be clearly observed before the flows
 273 saturate for large temperature differences.

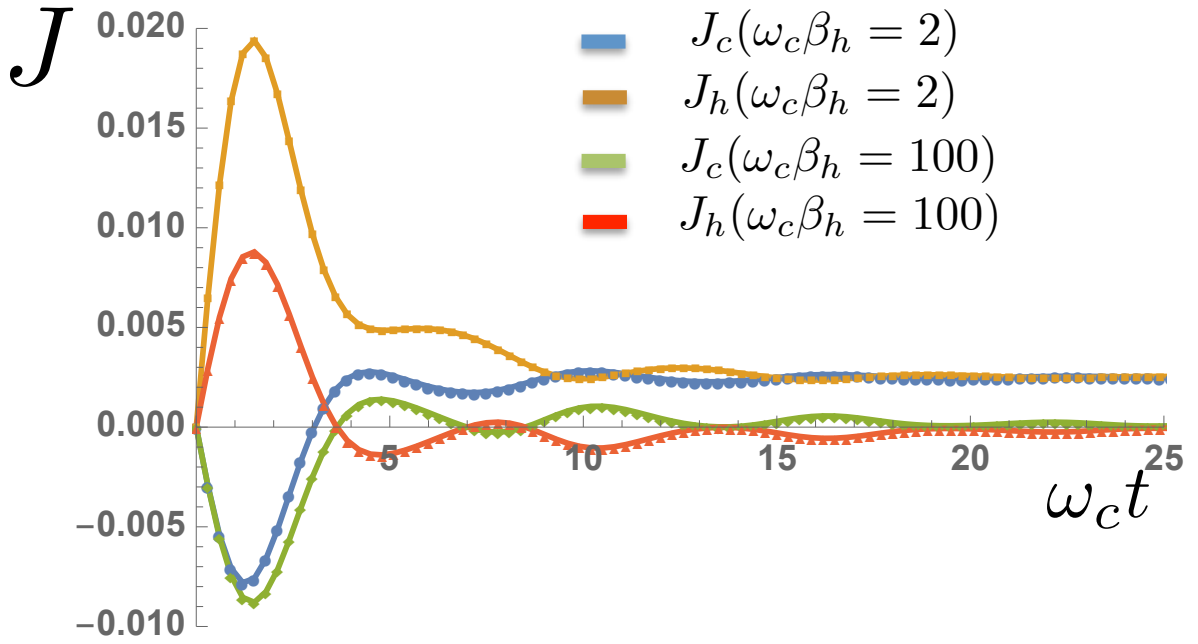


Figure 10. Heat flows into the cold bath (J_c) and out of the hot bath (J_h) as a function of time for varying hot bath temperatures and a fixed $\omega_c \beta_c = 100$.

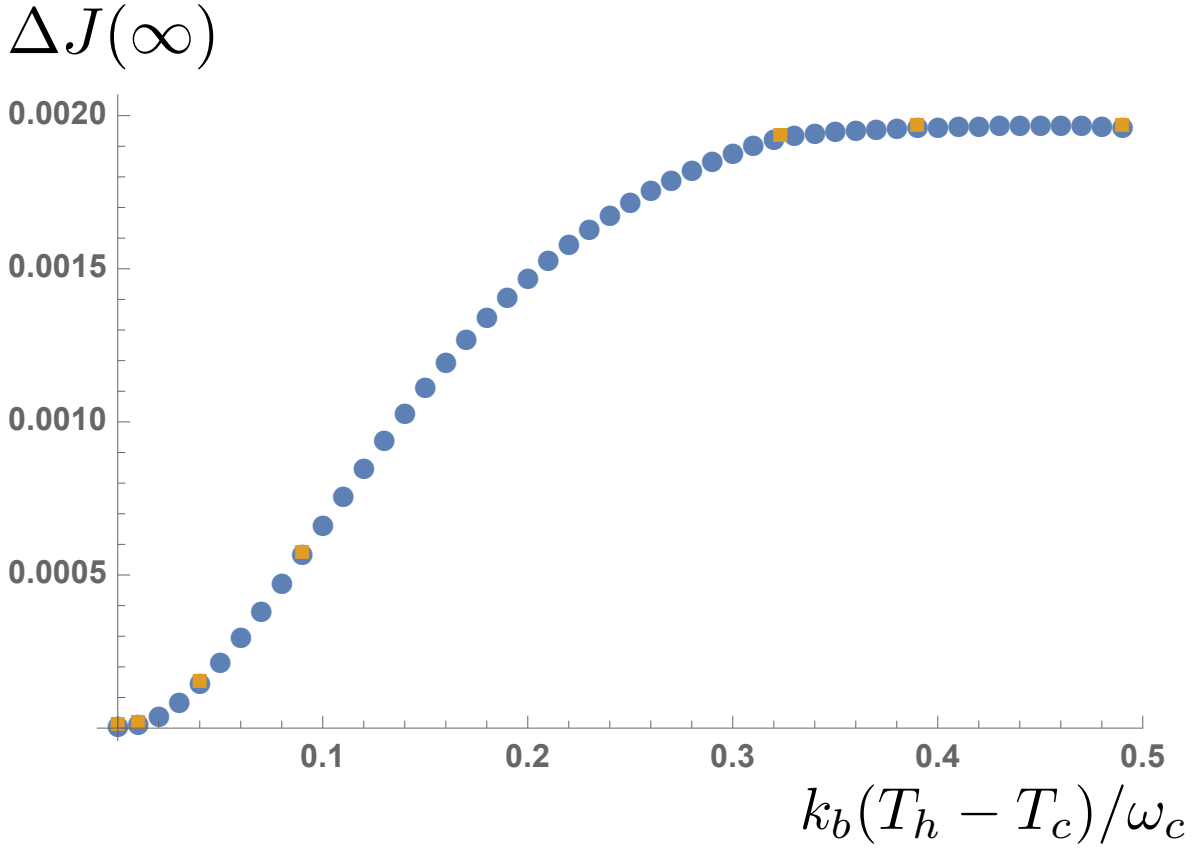


Figure 11. Net steady-state heat flux through the two-level system as a function of temperature difference for a fixed $\beta_c = 100$. Data extracted from MPS simulations (yellow squares) is compared with the analytical expression in the main text (blue dots).

274 3. Discussion

275 The results presented in Section 2 demonstrate that accurate reduced system behaviour in
 276 the spin-boson model can be obtained in the presence of both a single or two finite-temperature
 277 environments. Non-perturbative effects related to system-bath entanglement (polaronic dressing)
 278 are captured in transient relaxation and non-equilibrium steady states, and we have shown how the
 279 T-TEDOPA transformation provides direct information related to the energy and entanglement entropy
 280 flows in the environment. All of these results were obtained from pure wave function evolution of an
 281 initial zero-temperature (vacuum) state, and the onerous numerical cost of having to sample over a
 282 thermal distribution of initial states was entirely avoided.

283 However, we did note that the numerical resources required to obtain these results grew in an
 284 unbounded way as a function of simulation time. In the case of the one-bath SBM, Figure 6 shows
 285 that the total number of bosonic excitation grows approximately linearly in time and the growth rate
 286 increases with the bath temperature. The main panel showing the populations of the environment in
 287 frequency space shows that this growth is the result of growing populations at frequencies $\approx \pm\omega_0$. In
 288 Section 2.2 we made the observation that creating an excitation in a *negative* frequency mode allows
 289 the TLS to be excited with overall conservation of energy, and this is the process that accounts for the
 290 ‘heating’ expected of a finite-temperature bath. The constant growth of excitations in the environment
 291 can be seen to arise from the constant cycling of the heating process sketched in Figure 12 (a similar
 292 cycle for cooling also generates a net population of excitations). Here the creation of a negative
 293 frequency excitation (or hole) excites the TLS and then is de-excited by the creation of an excitation in
 294 the positive frequency environment.

295 Interestingly, this pair creation goes beyond populations: the dynamics of thermalization entangles
 296 the positive and negative frequency environments. This is perhaps unsurprising in the context of the

297 thermofield theory of De Vega *et al.* where the thermal entanglement properties of two-mode squeezed
 298 states are used to create an effective finite temperature environment from two zero-temperature baths
 299 [59]. However, for our open-system problem, it should be kept in mind that the 'dynamics' of the
 300 positive and - especially - the negative modes really only provide insight into the internal workings
 301 of the simulation. The modes and their populations are proxy (non-physical) degrees of freedom
 302 used to provide vacuum fluctuations that mimic the physical interactions of the system with a strictly
 303 positive-frequency harmonic bath at finite-temperature. However, a hopefully fruitful and more
 304 physical connection between the behaviour of the artificially extended environment inT-TEDOPA can
 305 be made to very recent developments in the theory of MPS and tensor networks for fermionic quantum
 306 transport. Here, non-equilibrium particle flows between reservoirs at different chemical potentials
 307 lead to the constant creation of entangled particle-hole pairs, leading to the exponential-in-time growth
 308 of MPS bond dimensions. However, Rams and Zwolak have recently demonstrated that a change
 309 in basis used for certain fermionic transport simulations can greatly suppress the rapid growth of
 310 numerical resources [60], and it would be very interesting to see how this might translate - or might to
 311 some extent already be implemented - in our current approach to bosonic heat flow problems. Finally,
 312 we also point out that rapid growth of bond dimensions and entanglement in non-equilibrium systems
 313 is potentially a problem for 1TDVP simulations, as these proceed at fixed bond-dimensions. Choosing
 314 large bond-dimensions may allow one to reach long times, but much of the simulation is likely to
 315 run slowly, as it will be using far more resources than are necessary for most of the time. In a recent
 316 development, Dunnett and Chin have proposed an adaptive version of 1TDVP that is able to change
 317 bond-dimensions during the course of a single simulation run, allowing the necessary resources to
 318 be deployed *as needed* [61]. We thus conclude that recent insights and computational development
 319 have opened a whole new domain of finite and multiple-temperature open system problems for wave
 320 function techniques, and that creating numerically efficient finite-temperature simulations will inspire
 321 further progress in tensor network theory, as applied to open systems.

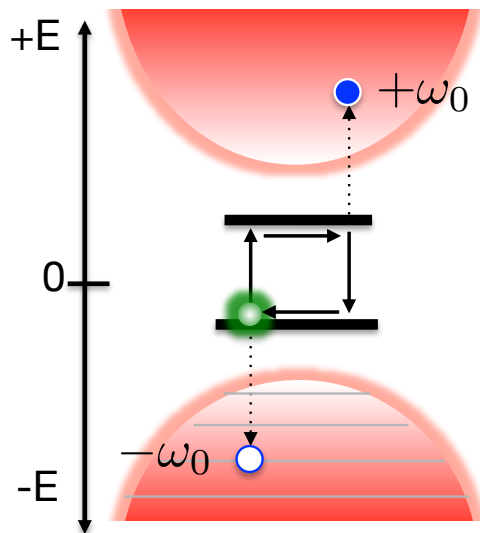


Figure 12. Due to the unbounded bosonic nature of the negative-frequency environment, thermal transitions within the TLS lead to a constant creation of correlated, particle-hole-like excitations in both environments with the same absolute energy ω_0 .

322 4. Materials and Methods

323 All numerical results have been obtained using software packages that are available at
324 <https://github.com/angusdunnett/MPSDynamics>. The benchmark data for the Ohmic Spin-Boson
325 Model can be found at [46].

326 **Author Contributions:** Conceptualisation, AWC; methodology, AJD & AWC; software, AJD; writing–original
327 draft preparation, AWC & AJD; All authors have read and agreed to the published version of the manuscript.

328 **Funding:** ADJ Acknowledges support from Ecole Doctorale Physique en Ile-de-France (EDPIF ED564. AWC is
329 partly supported by ANR project No. 195608/ACCEPT.

330 **Conflicts of Interest:** The authors declare no conflict of interest.

331 References

- 332 1. Tamascelli, D.; Smirne, A.; Lim, J.; Huelga, S.F.; Plenio, M.B. Efficient simulation of finite-temperature
333 open quantum systems. *Physical Review Letters* **2019**, *123*, 090402. arXiv: 1811.12418,
334 doi:10.1103/PhysRevLett.123.090402.
- 335 2. Weiss, U. *Quantum Dissipative Systems*, 4 ed.; WORLD SCIENTIFIC, 2012. doi:10.1142/8334.
- 336 3. Breuer, H.P.; Petruccione, F.; others. *The theory of open quantum systems*; Oxford University Press on Demand,
337 2002.
- 338 4. Acín, A.; Bloch, I.; Buhrman, H.; Calarco, T.; Eichler, C.; Eisert, J.; Esteve, D.; Gisin, N.; Glaser, S.J.; Jelezko,
339 F.; others. The quantum technologies roadmap: a European community view. *New Journal of Physics* **2018**,
340 *20*, 080201.
- 341 5. Gemmer, J.; Michel, M.; Mahler, G. *Quantum thermodynamics: Emergence of thermodynamic behavior within*
342 *composite quantum systems*; Vol. 784, Springer, 2009.
- 343 6. Kosloff, R.; Levy, A. Quantum Heat Engines and Refrigerators: Continuous Devices. *Annual Review of*
344 *Physical Chemistry* **2014**, *65*, 365–393. doi:10.1146/annurev-physchem-040513-103724.
- 345 7. Benenti, G.; Casati, G.; Saito, K.; Whitney, R. Fundamental aspects of steady-state conversion of heat to
346 work at the nanoscale. *Physics Reports* **2017**, *694*, 1–124. doi:10.1016/j.physrep.2017.05.008.
- 347 8. Elenewski, J.E.; Gruss, D.; Zwolak, M. Communication: Master equations for electron transport: The limits
348 of the Markovian limit. *The Journal of chemical physics* **2017**, *147*, 151101.
- 349 9. Thoss, M.; Evers, F. Perspective: Theory of quantum transport in molecular junctions. *The Journal of*
350 *chemical physics* **2018**, *148*, 030901.
- 351 10. Ishizaki, A.; Fleming, G.R. Unified treatment of quantum coherent and incoherent hopping dynamics
352 in electronic energy transfer: Reduced hierarchy equation approach. *The Journal of chemical physics* **2009**,
353 *130*, 234111.
- 354 11. Chin, A.; Prior, J.; Rosenbach, R.; Caycedo-Soler, F.; Huelga, S.F.; Plenio, M.B. The role of non-equilibrium
355 vibrational structures in electronic coherence and recoherence in pigment–protein complexes. *Nature*
356 *Physics* **2013**, *9*, 113–118.
- 357 12. Smith, S.L.; Chin, A.W. Ultrafast charge separation and nongeminate electron–hole recombination in
358 organic photovoltaics. *Physical Chemistry Chemical Physics* **2014**, *16*, 20305–20309.
- 359 13. Oviedo-Casado, S.; Prior, J.; Chin, A.; Rosenbach, R.; Huelga, S.; Plenio, M. Phase-dependent exciton
360 transport and energy harvesting from thermal environments. *Physical Review A* **2016**, *93*, 020102.
- 361 14. Chin, A.; Mangaud, E.; Atabek, O.; Desouter-Lecomte, M. Coherent quantum dynamics launched by
362 incoherent relaxation in a quantum circuit simulator of a light-harvesting complex. *Physical Review A* **2018**,
363 *97*, 063823.
- 364 15. Schröder, F.A.; Turban, D.H.; Musser, A.J.; Hine, N.D.; Chin, A.W. Tensor network simulation of
365 multi-environmental open quantum dynamics via machine learning and entanglement renormalisation.
366 *Nature communications* **2019**, *10*, 1–10.
- 367 16. Maguire, H.; Iles-Smith, J.; Nazir, A. Environmental nonadditivity and franck-condon physics in
368 nonequilibrium quantum systems. *Physical review letters* **2019**, *123*, 093601.
- 369 17. Wertnik, M.; Chin, A.; Nori, F.; Lambert, N. Optimizing co-operative multi-environment dynamics in a
370 dark-state-enhanced photosynthetic heat engine. *The Journal of chemical physics* **2018**, *149*, 084112.

- 371 18. Del Pino, J.; Schröder, F.A.; Chin, A.W.; Feist, J.; Garcia-Vidal, F.J. Tensor network simulation of
372 polaron-polaritons in organic microcavities. *Physical Review B* **2018**, *98*, 165416.
- 373 19. Weiss, U. *Quantum dissipative systems*; Vol. 13, World scientific, 2012.
- 374 20. Strathearn, A.; Kirton, P.; Kilda, D.; Keeling, J.; Lovett, B.W. Efficient non-Markovian quantum
375 dynamics using time-evolving matrix product operators. *Nature Communications* **2018**, *9*, 3322.
376 doi:10.1038/s41467-018-05617-3.
- 377 21. Topaler, M.; Makri, N. Quantum rates for a double well coupled to a dissipative bath: Accurate path integral
378 results and comparison with approximate theories. *The Journal of chemical physics* **1994**, *101*, 7500–7519.
- 379 22. Prior, J.; Chin, A.W.; Huelga, S.F.; Plenio, M.B. Efficient simulation of strong system-environment
380 interactions. *Physical review letters* **2010**, *105*, 050404.
- 381 23. Oviedo-Casado, S.; Prior, J.; Chin, A.W.; Rosenbach, R.; Huelga, S.F.; Plenio, M.B. Phase-dependent
382 exciton transport and energy harvesting from thermal environments. *Phys. Rev. A* **2016**, *93*, 020102.
383 doi:10.1103/PhysRevA.93.020102.
- 384 24. Somoza, A.D.; Marty, O.; Lim, J.; Huelga, S.F.; Plenio, M.B. Dissipation-Assisted Matrix Product
385 Factorization. *Phys. Rev. Lett.* **2019**, *123*, 100502. doi:10.1103/PhysRevLett.123.100502.
- 386 25. Lindner, C.J.; Kugler, F.B.; Meden, V.; Schoeller, H. Renormalization group transport theory for open
387 quantum systems: Charge fluctuations in multilevel quantum dots in and out of equilibrium. *Physical*
388 *Review B* **2019**, *99*, 205142.
- 389 26. Wang, H.; Shao, J. Quantum Phase Transition in the Spin-Boson Model: A Multilayer Multiconfiguration
390 Time-Dependent Hartree Study. *The Journal of Physical Chemistry A* **2019**, *123*, 1882–1893.
- 391 27. Haegeman, J.; Lubich, C.; Oseledets, I.; Vandereycken, B.; Verstraete, F. Unifying time evolution
392 and optimization with matrix product states. *Physical Review B* **2016**, *94*, 165116. arXiv: 1408.5056,
393 doi:10.1103/PhysRevB.94.165116.
- 394 28. Haegeman, J.; Cirac, J.I.; Osborne, T.J.; Pižorn, I.; Verschelde, H.; Verstraete, F. Time-Dependent
395 Variational Principle for Quantum Lattices. *Physical Review Letters* **2011**, *107*, 070601.
396 doi:10.1103/PhysRevLett.107.070601.
- 397 29. Schröder, F.A.Y.N.; Chin, A.W. Simulating open quantum dynamics with time-dependent variational
398 matrix product states: Towards microscopic correlation of environment dynamics and reduced system
399 evolution. *Phys. Rev. B* **2016**, *93*, 075105. doi:10.1103/PhysRevB.93.075105.
- 400 30. Gonzalez-Ballester, C.; Schröder, F.A.Y.N.; Chin, A.W. Uncovering nonperturbative dynamics of the
401 biased sub-Ohmic spin-boson model with variational matrix product states. *Phys. Rev. B* **2017**, *96*, 115427.
402 doi:10.1103/PhysRevB.96.115427.
- 403 31. Tamascelli, D.; Smirne, A.; Huelga, S.; Plenio, M. Nonperturbative Treatment of non-Markovian Dynamics
404 of Open Quantum Systems. *Physical Review Letters* **2018**, *120*, 030402. doi:10.1103/PhysRevLett.120.030402.
- 405 32. Wilhelm, F.; Kleff, S.; Von Delft, J. The spin-boson model with a structured environment: a comparison of
406 approaches. *Chemical physics* **2004**, *296*, 345–353.
- 407 33. Schulze, J.; Kuhn, O. Explicit correlated exciton-vibrational dynamics of the FMO complex. *The Journal of*
408 *Physical Chemistry B* **2015**, *119*, 6211–6216.
- 409 34. Mendive-Tapia, D.; Mangaud, E.; Firmino, T.; de la Lande, A.; Desouter-Lecomte, M.; Meyer, H.D.; Gatti, F.
410 Multidimensional quantum mechanical modeling of electron transfer and electronic coherence in plant
411 cryptochromes: The role of initial bath conditions. *The Journal of Physical Chemistry B* **2018**, *122*, 126–136.
- 412 35. May, V.; Kühn, O. *Charge and energy transfer dynamics in molecular systems*; John Wiley & Sons, 2008.
- 413 36. Mukamel, S. *Principles of nonlinear optical spectroscopy*; Vol. 6, Oxford university press New York, 1995.
- 414 37. Alvermann, A.; Fehske, H. Sparse polynomial space approach to dissipative quantum systems: Application
415 to the sub-ohmic spin-boson model. *Physical review letters* **2009**, *102*, 150601.
- 416 38. Binder, R.; Burghardt, I. First-principles quantum simulations of exciton diffusion on a minimal
417 oligothiophene chain at finite temperature. *Faraday Discussions* **2019**, *221*, 406–427.
- 418 39. Jiang, T.; Li, W.; Ren, J.; Shuai, Z. Finite Temperature Dynamical Density Matrix Renormalization Group
419 for Spectroscopy in Frequency Domain. *The Journal of Physical Chemistry Letters* **2020**, *11*, 3761–3768. PMID:
420 32316732, doi:10.1021/acs.jpcllett.0c00905.
- 421 40. Musser, A.J.; Liebel, M.; Schnedermann, C.; Wende, T.; Kehoe, T.B.; Rao, A.; Kukura, P. Evidence for conical
422 intersection dynamics mediating ultrafast singlet exciton fission. *Nature Physics* **2015**, *11*, 352–357.

- 423 41. Schnedermann, C.; Lim, J.M.; Wende, T.; Duarte, A.S.; Ni, L.; Gu, Q.; Sadhanala, A.; Rao, A.; Kukura,
424 P. Sub-10 fs time-resolved vibronic optical microscopy. *The journal of physical chemistry letters* **2016**,
425 7, 4854–4859.
- 426 42. Schnedermann, C.; Alvertis, A.M.; Wende, T.; Lukman, S.; Feng, J.; Schröder, F.A.; Turban, D.H.; Wu, J.;
427 Hine, N.D.; Greenham, N.C.; others. A molecular movie of ultrafast singlet fission. *Nature communications*
428 **2019**, 10, 1–11.
- 429 43. Chin, A.W.; Rivas, Á.; Huelga, S.F.; Plenio, M.B. Exact mapping between system-reservoir quantum
430 models and semi-infinite discrete chains using orthogonal polynomials. *Journal of Mathematical Physics*
431 **2010**, 51, 092109.
- 432 44. Prior, J.; de Vega, I.; Chin, A.W.; Huelga, S.F.; Plenio, M.B. Quantum dynamics in photonic crystals. *Physical*
433 *Review A* **2013**, 87, 013428. arXiv: 1205.2897, doi:10.1103/PhysRevA.87.013428.
- 434 45. Chin, A.W.; Rivas, A.; Huelga, S.F.; Plenio, M.B. Exact mapping between system-reservoir quantum
435 models and semi-infinite discrete chains using orthogonal polynomials. *Journal of Mathematical Physics*
436 **2010**, 51, 092109. arXiv: 1006.4507, doi:10.1063/1.3490188.
- 437 46. Chin, A.; Dunnett, A. Real-time benchmark dynamics of the Ohmic Spin- Boson Model computed
438 with Time-Dependent Variational Matrix Product States. (TDVMPS) coupling strength and temperature
439 parameter space **2020**. doi:10.5281/zenodo.4352729.
- 440 47. Silbey, R.; Harris, R.A. Variational calculation of the dynamics of a two level system interacting with a
441 bath. *The Journal of Chemical Physics* **1984**, 80, 2615–2617. doi:10.1063/1.447055.
- 442 48. Blunden-Codd, Z.; Bera, S.; Bruognolo, B.; Linden, N.O.; Chin, A.W.; Von Delft, J.; Nazir, A.; Florens, S.
443 Anatomy of quantum critical wave functions in dissipative impurity problems. *Physical Review B* **2017**,
444 95, 085104.
- 445 49. Florens, S.; Freyn, A.; Venturelli, D.; Narayanan, R. Dissipative spin dynamics near a quantum critical
446 point: Numerical renormalization group and Majorana diagrammatics. *Physical Review B* **2011**, 84, 155110.
- 447 50. Bruognolo, B.; Weichselbaum, A.; Guo, C.; von Delft, J.; Schneider, I.; Vojta, M. Two-bath spin-boson model:
448 Phase diagram and critical properties. *Physical Review B* **2014**, 90, 245130.
- 449 51. Nielsen, M.A.; Chuang, I. Quantum computation and quantum information, 2002.
- 450 52. Dubi, Y.; Di Ventra, M. *Colloquium* : Heat flow and thermoelectricity in atomic and molecular junctions.
451 *Reviews of Modern Physics* **2011**, 83, 131–155. doi:10.1103/RevModPhys.83.131.
- 452 53. Dhar, A. Heat transport in low-dimensional systems. *Advances in Physics* **2008**, 57, 457–537.
453 doi:10.1080/00018730802538522.
- 454 54. Guo, C.; Weichselbaum, A.; vonDelft, J.; Vojta, M. Critical and Strong-Coupling Phases
455 in One- and Two-Bath Spin-Boson Models. *Physical Review Letters* **2012**, 108, 160401.
456 doi:10.1103/PhysRevLett.108.160401.
- 457 55. Zhou, N.; Chen, L.; Xu, D.; Chernyak, V.; Zhao, Y. Symmetry and the critical phase of
458 the two-bath spin-boson model: Ground-state properties. *Physical Review B* **2015**, 91, 195129.
459 doi:10.1103/PhysRevB.91.195129.
- 460 56. Bruognolo, B.; Weichselbaum, A.; Guo, C.; von Delft, J.; Schneider, I.; Vojta, M. Two-bath spin-boson model:
461 Phase diagram and critical properties. *Physical Review B* **2014**, 90, 245130. doi:10.1103/PhysRevB.90.245130.
- 462 57. Segal, D.; Nitzan, A. Spin-Boson Thermal Rectifier. *Physical Review Letters* **2005**, 94, 034301.
463 doi:10.1103/PhysRevLett.94.034301.
- 464 58. Chen, T.; Balachandran, V.; Guo, C.; Poletti, D. Steady state quantum transport through an anharmonic
465 oscillator strongly coupled to two heat reservoirs. *arXiv:2004.05017 [cond-mat]* **2020**. arXiv: 2004.05017.
- 466 59. de Vega, I.; Bañuls, M.C. Thermofield-based chain-mapping approach for open quantum systems. *Physical*
467 *Review A* **2015**, 92, 052116. doi:10.1103/PhysRevA.92.052116.
- 468 60. Rams, M.M.; Zwolak, M. Breaking the Entanglement Barrier: Tensor Network Simulation of Quantum
469 Transport. *Phys. Rev. Lett.* **2020**, 124, 137701. doi:10.1103/PhysRevLett.124.137701.
- 470 61. Dunnett, A.J.; Chin, A.W. Dynamically Evolving Bond-Dimensions within the one-site
471 Time-Dependent-Variational-Principle method for Matrix Product States: Towards efficient simulation of
472 non-equilibrium open quantum dynamics, 2020, [arXiv:quant-ph/2007.13528].

475 © 2020 by the authors. Submitted to *Journal Not Specified* for possible open access
476 publication under the terms and conditions of the Creative Commons Attribution (CC BY) license
477 (<http://creativecommons.org/licenses/by/4.0/>).